

Supporting Information

Robust Anti-Icing Surfaces Based on Dual Functionality – Microstructurally-Induced Ice Shedding with Superimposed Nanostructurally-Enhanced Water Shedding

Michael J. Wood, Gregory Brock, Juliette Debray, Phillip Servio, and
Anne-Marie Kietzig*

*Department of Chemical Engineering, McGill University,
Montréal, Québec, Canada, H3A 0C5*

E-mail: anne.kietzig@mcgill.ca

1 Wetting Transitions on Laser Micromachined Metals

Laser-micromachined metals are known to undergo a hydrophilic-to-hydrophobic surface chemistry transition upon exposure to lab air in the weeks following irradiation.^{1,2} A freshly irradiated metal possesses a hydroxylated surface chemistry which is initially free of organic adsorbates, thus presenting with high hydrophilicity.³ Over time, on the order of 3-4 weeks for simple exposure to ambient laboratory air, organic compounds from the air adsorb on the surface, creating a hydrophobic surface chemistry. Many researchers have found a strong correlation with increased carbon content on their surfaces and increased water contact angles with time.^{1,4-8} The kinetics of this transition in chemistry are not yet known, but the general trends of the Arrhenius relationship hold; increased temperatures and pressures increase the rate of transition.⁹⁻¹² The level of humidity in the ambient air also affects the rate of this wetting transition due to the competition in adsorption of water versus organic molecules.^{4,13-15} These environmental factors help to explain the differences seen in the time necessary after irradiation for the biomimetic surfaces to reach their maximum hydrophobicity. In Figure 3(b), the 200x1400 wire cloth decorated with hydrophobic LIPSS had not yet reached its maximum hydrophobicity through adsorption of hydrocarbons from the lab air before experimentation had commenced. This surface presented with a receding contact angle of only $52 \pm 10^\circ$ and thus cannot be considered water shedding at ice removal cycle 0. Likely caused by the actual composition and humidity of the laboratory air on the day of, and after fabrication, this specific surface evidently took slightly longer to reach its maximum hydrophobicity than the 325x2300 and 400x2800 wire cloths decorated with hydrophobic LIPSS. In fact, Figure 3(b) shows that maximum hydrophobicity is reached after the time taken to perform the first ice removal cycle. There were approximately 24 hours between the goniometric measurement taken at ice removal cycle 0 and ice removal cycle 1. After the first 24 hours of experimentation (ice removal cycle 1 onward), there is no further change in wettability on the 200x1400 wire cloth decorated with hydrophobic LIPSS, or indeed any of the biomimetic wire cloths.

The flat monolithic stainless-steel sample decorated with hydrophilic LIPSS similarly presents with slightly increasing apparent contact angles with time in Figure 3(c) despite us having stored this substrate in reverse osmosis water between experiments. The average apparent advancing contact angle increased to $64 \pm 5^\circ$ by the time we had performed the 5 ice removal cycles, and goniometric measurements between them. Evidently the time taken to perform these measurements offered enough exposure to the lab air to adsorb sufficient carbonaceous species to induce a nearly 20° increase in the apparent advancing contact angle.

To explore further the possible relationship between apparent advancing contact angle and ice adhesion strength, we fabricated a second flat stainless-steel surface decorated with initially hydrophilic LIPSS and stored this sample in air between ice adhesion and goniometric measurements. In doing so, we provoked a wider change in surface chemistry and manifested apparent advancing water contact angles. In Figure S1, it can be seen that this surface undergoes a transition in apparent advancing water contact angle from $27 \pm 3^\circ$ to $86 \pm 12^\circ$ over the time it took to perform the 5 ice removal cycles (approximately 5 days). However, there is no corresponding increasing or decreasing trend in measured ice adhesion strength. This observation matches well what we report in Figure 5 of the manuscript, that wettability under ambient conditions and ice adhesion strength are not correlated.

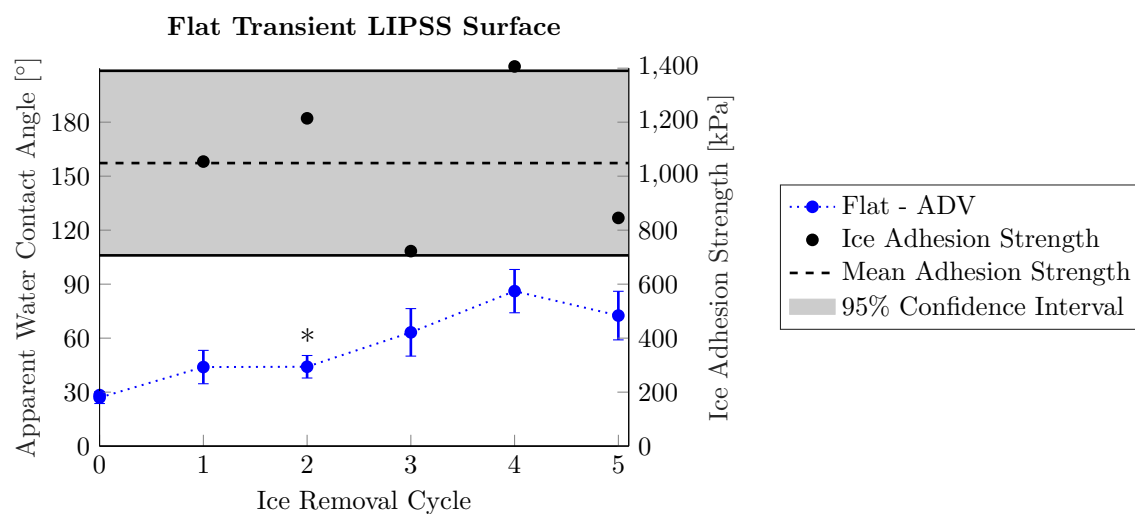


Figure S1: The dynamic apparent water contact angles alongside the ice adhesion strength for each de-icing cycle measured on the hydrophilic LIPSS-decorated flat surface stored in ambient lab air between measurements. * sessile water contact angle data plotted at this point as equipment malfunction made dynamic data unavailable.

2 Peak Dislodging Force Data

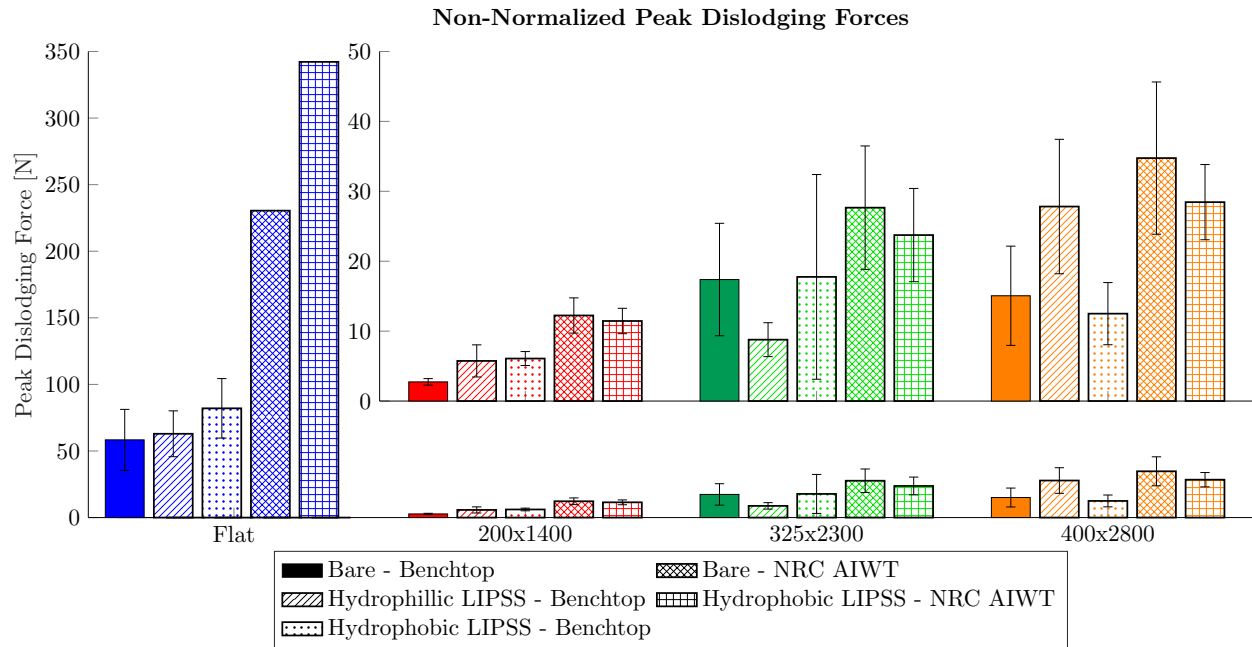


Figure S2: Average peak force required to dislodge ice from all experimental surfaces. Error bars represent 95% confidence intervals on the mean.

3 Wire Cloth Surface Area Measurement

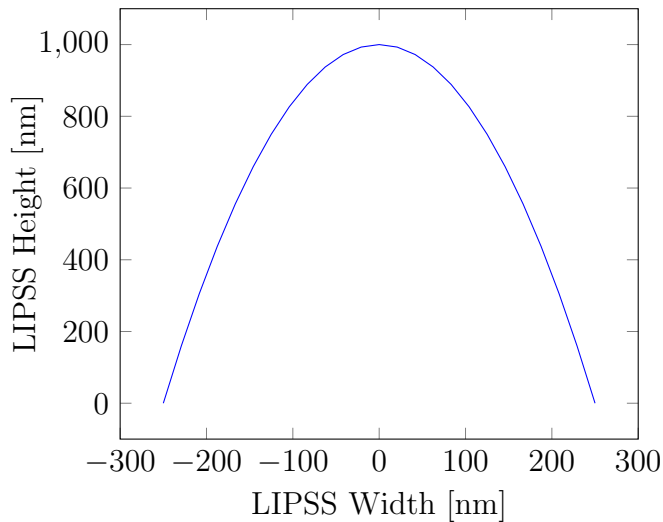
3.1 Methodology for Bare Cloths

Micro-tomography analyses of the three bare wire cloth substrates were performed using a *Xradia Versa 520* 3D X-ray microscope (Carl Zeiss, AG., Jena, TH, Germany). The collected image slices were reconstructed and segmented using *Dragonfly* (Object Research Systems, Inc., Montréal, QC, Canada) in order to extract the total surface area of the 3D-microstructural networks.

3.2 Methodology for LIPSS

3.2.1 Dimension of LIPSS

- LIPSS formed on flat, polished stainless-steel have a periodicity ≈ 500 nm, matching what is quoted in literature;
- The height of each ripple has been reported to be ≈ 1000 nm;²
- Further, the cross-section of the ripples are assumed to be parabolic.



3.2.2 Arc Length of a Parabola

The formula for the parabolic cross-section is given by:

$$f(x) = 1000 - 0.016x^2 \quad (1)$$

for $-250 \leq x \leq 250$.

Arc length can be computed by:

$$\text{Arc Length} = \int_{x=a}^b \sqrt{1 + (f'(x))^2} dx \quad (2)$$

where:

$$f'(x) = -0.032x \quad (3)$$

therefore, we need to compute the following integral:

$$\text{Arc Length} = \int_{x=-250}^{250} \sqrt{1 + 0.001024x^2} dx \approx 2102 \text{ nm} \quad (4)$$

3.2.3 Surface Area of LIPSS

- Assuming the parabolic ripples abut to one another directly, 1 mm of surface which has been laser-irradiated will be decorated with:

$$\frac{1000000 \text{ nm}}{500 \text{ nm}} \approx 2000 \text{ ripples} \quad (5)$$

- Therefore, in 1 mm^2 , the total surface area of the LIPSS-decorated surface will be:

$$(2000 \text{ ripples}) \cdot \left(2102 \frac{\text{nm}}{\text{ripple}} \right) \cdot (1000000 \text{ nm}) = 4.21 \times 10^{12} \text{ nm}^2 \quad (6)$$

- Thus, the total surface area of the LIPSS-decorated surfaces, compared to the geometric surface area, is approximately:

$$\frac{4.21 \mu\text{m}^2}{\mu\text{m}^2} \quad (7)$$

3.3 Tabulated Surface Areas

Surface	Total Area vs. Geometric [μm / μm]
Flat Bare	1
Flat LIPSS	4.21
200x1400 Bare	3.71
200x1400 LIPSS	15.62
325x2300 Bare	3.79
325x2300 LIPSS	15.96
400x2800 Bare	3.70
400x2800 LIPSS	15.58

References

- (1) Kietzig, A.-M.; Hatzikiriakos, S. G.; Englezos, P. Patterned Superhydrophobic Metallic Surfaces. *Langmuir* **2009**, *25*, 4821–4827.
- (2) Bonse, J. Quo Vadis LIPSS?—Recent and Future Trends on Laser-Induced Periodic Surface Structures. *Nanomaterials* **2020**, *10*, 1950.
- (3) Long, J.; Zhong, M.; Zhang, H.; Fan, P. Superhydrophilicity to Superhydrophobicity Transition of Picosecond Laser Microstructured Aluminum in Ambient Air. *J. Colloid Interface Sci.* **2015**, *441*, 1–9.
- (4) Kietzig, A.-M.; Negar Mirvakili, M.; Kamal, S.; Englezos, P.; Hatzikiriakos, S. G. Laser-Patterned Super-Hydrophobic Pure Metallic Substrates: Cassie to Wenzel Wetting Transitions. *J. Adhes. Sci. Technol.* **2011**, *25*, 2789–2809.
- (5) Tang, M.; Shim, V.; Pan, Z. Y.; Choo, Y. S.; Hong, M. H. Laser Ablation of Metal Substrates for Super-hydrophobic Effect. *J. Laser Micro Nanoeng.* **2011**, *6*, 6–9.
- (6) Bizi-bandoki, P.; Valette, S.; Audouard, E.; Benayoun, S. Time Dependency of the Hydrophilicity and Hydrophobicity of Metallic Alloys Subjected to Femtosecond Laser Irradiations. *Appl. Surf. Sci.* **2013**, *273*, 399–407.
- (7) Yan, H.; Abdul Rashid, M. R. B.; Khew, S. Y.; Li, F.; Hong, M. Wettability Transition of Laser Textured Brass Surfaces Inside Different Mediums. *Appl. Surf. Sci.* **2018**, *427*, 369–375.
- (8) Gregorčič, P.; Conradi, M.; Hribar, L.; Hočevar, M. Long-Term Influence of Laser-Processing Parameters on (Super)hydrophobicity Development and Stability of Stainless-Steel Surfaces. *Materials* **2018**, *11*, 2240.
- (9) Chun, D.-M.; Ngo, C.-V.; Lee, K.-M. Fast Fabrication of Superhydrophobic Metallic

- Surface Using Nanosecond Laser Texturing and Low-Temperature Annealing. *CIRP Annals* **2016**, *65*, 519–522.
- (10) Ngo, C.-V.; Chun, D.-M. Fast Wettability Transition from Hydrophilic to Superhydrophobic Laser-Textured Stainless Steel Surfaces Under Low-Temperature Annealing. *Appl. Surf. Sci.* **2017**, *409*, 232–240.
- (11) Ngo, C.-V.; Chun, D.-M. Control of Laser-Ablated Aluminum Surface Wettability to Superhydrophobic or Superhydrophilic Through Simple Heat Treatment or Water Boiling Post-Processing. *Appl. Surf. Sci.* **2018**, *435*, 974–982.
- (12) Ngo, C.-V.; Chun, D.-M. Effect of Heat Treatment Temperature on the Wettability Transition from Hydrophilic to Superhydrophobic on Laser-Ablated Metallic Surfaces. *Adv. Eng. Mater.* **2018**, *20*, 1701086.
- (13) Cardoso, J. T.; Garcia-Girón, A.; Romano, J. M.; Huerta-Murillo, D.; Jagdheesh, R.; Walker, M.; Dimov, S. S.; Ocaña, J. L. Influence of Ambient Conditions on the Evolution of Wettability Properties of an IR-, ns-Laser Textured Aluminium Alloy. *RSC Adv.* **2017**, *7*, 39617–39627.
- (14) Jagdheesh, R.; Diaz, M.; Marimuthu, S.; Ocana, J. L. Robust Fabrication of μ -Patterns with Tunable and Durable Wetting Properties: Hydrophilic to Ultrahydrophobic via a Vacuum Process. *J. Mater. Chem. A* **2017**, *5*, 7125–7136.
- (15) White, B.; Sarkar, A.; Kietzig, A.-M. Fog-Harvesting Inspired by the *Stenocara* Beetle—An Analysis of Drop Collection and Removal from Biomimetic Samples with Wetting Contrast. *Appl. Surf. Sci.* **2013**, *284*, 826–836.